Evidence for polaron conduction in nanostructured manganese ferrite

2008 J. Phys. D: Appl. Phys. 41 185005

(http://iopscience.iop.org/0022-3727/41/18/185005)

J. Phys. D: Appl. Phys. **41** (2008) 185005 (9pp) doi:10.1088/0022-3727/41/18/185005

Evidence for polaron conduction in nanostructured manganese ferrite

E Veena Gopalan[1], K A Malini[2], S Saravanan[3], D Sakthi Kumar[4], Yasuhiko Yoshida[4] and M R Anantharaman[1]

[1] Department of Physics, Cochin University of Science and Technology, Cochin 682 022, Kerala, India
[2] Department of Physics, Vimala College, Thrissur 680 009, Kerala, India
[3] Department of Materials Engineering, Indian Institute of Science, Bangalore 560 012, Karnataka, India
[4] Bio-Nano Electronics Research Centre, Department of Applied Chemistry, Toyo University, Japan

E-mail: mraiyer@gmail.com (M R Anantharaman)

Received 19 April 2008, in final form 24 July 2008
Published 29 August 2008
Online at stacks.iop.org/JPhysD/41/185005

Abstract

Nanoparticles of manganese ferrite were prepared by the chemical co-precipitation technique. The dielectric parameters, namely, real and imaginary dielectric permittivity (ε' and ε''), ac conductivity (σ_{ac}) and dielectric loss tangent ($\tan\delta$), were measured in the frequency range of 100 kHz–8 MHz at different temperatures. The variations of dielectric dispersion (ε') and dielectric absorption (ε'') with frequency and temperature were also investigated. The variation of dielectric permittivity with frequency and temperature followed the Maxwell–Wagner model based on interfacial polarization in consonance with Koops phenomenological theory. The dielectric loss tangent and hence ε'' exhibited a relaxation at certain frequencies and at relatively higher temperatures. The dispersion of dielectric permittivity and broadening of the dielectric absorption suggest the possibility of a distribution of relaxation time and the existence of multiple equilibrium states in manganese ferrite. The activation energy estimated from the dielectric relaxation is found to be high and is characteristic of polaron conduction in the nanosized manganese ferrite. The ac conductivity followed a power law dependence $\sigma_{ac} = B\omega^n$ typical of charge transport assisted by a hopping or tunnelling process. The observed minimum in the temperature dependence of the frequency exponent n strongly suggests that tunnelling of the large polarons is the dominant transport process.

(Some figures in this article are in colour only in the electronic version)

1. Introduction

The electrical properties of materials in the nanoregime are totally different when compared with their bulk counterparts in the micrometre regime. The modification of the dielectric properties upon particle size reduction is attributed to a variety of reasons, namely particle size, shape and boundaries. Though these modified dielectric properties of the nanostructures have been effectively used in various dielectric-based applications such as capacitors, electronic memories and optical filters, the level of understanding of the dielectric properties of nanosystems is far from being satisfactory, from both a qualitative and a quantitative perspective.

Ferrites assume special significance in the field of electronics and telecommunication industry because of their novel electrical properties which make them useful in radiofrequency circuits, high quality filters, rod antennas, transformer cores, read/write heads for high speed digital tapes and other devices [1–3]. Properties of ferrites were found to be sensitive to their composition and microstructure, which in turn are sensitive to their processing conditions. Nanoparticles of spinel ferrites possessing unique dielectric properties are effectively used for specific applications. Nanoparticles of $MnFe_2O_4$ attracted much attention because of their potential as contrast enhancing agents in magnetic resonance imaging, as precursors for ferrofluids and in magnetocaloric refrigeration [4].

$MnFe_2O_4$ has a face centred cubic structure with two types of lattice sites: (1) a tetrahedral site A formed by four oxygen anions and (2) an octahedral lattice site B formed by six oxygen anions [5]. In the bulk form $MnFe_2O_4$ is found to be 20% inverse with a stoichiometry of $Mn_{0.8}Fe_{0.2}$ $[Mn_{0.2}$ $Fe_{0.8}]O_4$

where cations in brackets occupy octahedral sites. But a higher inversion up to 60% was reported in nanosized manganese ferrite [6]. Different characterization techniques such as neutron diffraction, Mossbauer spectroscopy and nuclear magnetic resonance spectroscopy were used to determine the cation distribution in these nanosystems [7]. Neutron diffraction experiments showed that the $MnFe_2O_4$ prepared using wet chemical methods was 33% normal, which gave a distribution of $Mn_{0.33}Fe_{0.67}[Mn_{0.67}Fe_{1.33}]O_4$ [6]. In the nanoregime, manganese ferrite was found to undergo a cation rearrangement and the multiple oxidation state of Mn species was found to influence the structural magnetic and electrical properties to a great extent [8, 9]. Different techniques such as electron energy loss spectroscopy (EELS) [10], x-ray absorption near edge structure (XANES) and extended x-ray absorption fine structure (EXAFS) were used to investigate the oxidation state of Mn in manganese ferrite. Denecke *et al* [11] reported the presence of trivalent manganese and divalent iron in precipitated $MnFe_2O_4$ nanoparticles, and a large Jahn–Teller elongation of the Mn (III) octahedra was also noticed.

There are numerous reports with regard to the finite size effects on the structural and magnetic properties of manganese ferrite nanoparticles [12, 13]. However there exist only a few systematic studies on the dielectric properties in the nanoregime. The dielectric properties of ferrites are normally characteristic of hopping of electrons or polarons between cationic sites. Thus the cation distribution and also the oxidation states of the cations play a dominant role in electrical conduction. Hence, the study of dielectric properties can be thought of as an effective tool to investigate the finite size effects on the conduction mechanism in ferrites.

Phase pure manganese ferrite nanoparticles were synthesized by the chemical co-precipitation method. The variation of ε', ε'', $\tan\delta$ and σ_{ac} with frequency and temperature were studied. They were modelled with existing theories of dielectric polarization.

2. Experimental

$MnFe_2O_4$ nanoparticles were synthesized by wet chemical co-precipitation. Aqueous solutions of 1 molar manganese chloride ($MnCl_2 \cdot 4H_2O$) and 2 molar ferric chloride ($FeCl_3$ anhydrous) were mixed to form a solution. This solution was poured quickly into a boiling 10 M NaOH solution diluted in 1800 ml of water under vigorous stirring. The formation of precipitate was found to be in the pH range of 12.5–13. The solution was kept at 90 °C for 40 min under vigorous stirring. The precipitate was washed several times with distilled water, then filtered and dried in an oven.

The sample was characterized by using x-ray powder diffractometer (Rigaku Dmax-C) using Cu-Kα radiation (λ = 1.5405 Å). The lattice parameter was calculated assuming cubic symmetry. The average crystallite size was estimated by employing the Debye–Scherrer formula. The particle size of the samples was estimated by subjecting them to transmission electron microscopic studies (Jeol JEM-2200 FS). Hysteresis loop parameters at room temperature were evaluated by using a vibrating sample magnetometer (model: EG&G PAR 4500). High resolution scanning electron microscopy was employed to check the morphology of the pelletized samples (JSM-6335 FESEM).

Dielectric measurements were carried out on these samples using a home-made dielectric cell and an HP 4285 LCR meter in the frequency range 100 kHz–8 MHz over a temperature range of 303–403 K. The principle of parallel plate capacitor was employed for the evaluation of permittivity. The data acquisition was automated by interfacing the LCR meter with a virtual instrumentation package called LABVIEW (National Instruments). The dielectric permittivity of the sample was calculated using the relation

$$C = \frac{\varepsilon_0 \varepsilon_r A}{d}, \tag{1}$$

where C is the capacitance of the parallel plate capacitor with thickness d and area of cross section A, ε_0 the permittivity of free space and ε_r the relative permittivity of the dielectric material.

The dielectric permittivity is complex in nature and of the form $\varepsilon = (\varepsilon' - j\varepsilon'')$, where the imaginary part ε'' indicates the absorption in the medium. The loss factor or dissipation factor in any dielectric is given by the relation

$$\tan\delta = \frac{\varepsilon''(\omega)}{\varepsilon'(\omega)}. \tag{2}$$

From the loss factor ($\tan\delta$) and the real part of the dielectric constant (ε'), the ac conductivity (σ_{ac}) of these samples can be evaluated using the relation

$$\sigma_{ac} = 2\pi f \tan\delta \varepsilon_0 \varepsilon_r, \tag{3}$$

where f is the frequency of the applied field. The details are given elsewhere [14].

3. Results and discussion

3.1. Structural and magnetic characterization

The XRD pattern of $MnFe_2O_4$ is depicted in figure 1 and is typical of a spinel structure. The average size of the crystallite, calculated using the Debye–Scherrer formula was found to be 29 nm. The lattice parameter a was found to be 8.497 Å. It should be noted that the lattice parameter of the bulk manganese ferrite is 8.515 Å (JCPDS—file no: 73-1964). The observed deviation of the lattice parameter can be attributed to the rearrangement of cations in the nano $MnFe_2O_4$. The presence of Mn as Mn^{3+} leading to Jahn–Teller distortion in the MnO_6 octahedra [11] could also be one of the reasons for the observed decrease in the lattice parameter.

Figures 2(a) and (b) depict the TEM and HRTEM micrographs of $MnFe_2O_4$. The average particle size is estimated to be 28 nm, which is consistent with that obtained from line broadening analysis of x-ray diffraction. The lattice planes are clearly visible in the HRTEM images.

Scanning electron micrographs of these samples are depicted in figure 3. It can be seen that the grains are uniformly sized and are in the nanoregime.

The hysteresis loop of manganese ferrite recorded at room temperature is shown in figure 4. The saturation magnetization M_s was found to be 57 emu g^{-1}, which is lower than that of bulk $MnFe_2O_4$ (80 emu g^{-1}). The coercivity and magnetic remanence values were found to be 39 Oe and 4.66 emu g^{-1}, respectively.

All these are definite deviations from the corresponding bulk values and point to the existence of a metastable cation distribution which can give rise to different exchange interactions and will be manifested in the form of modified magnetic properties. Besides, the existence of Mn^{3+} ions ($4\,\mu_B$) with lower magnetic moment can result in reduced magnetization.

3.2. Dielectric properties

3.2.1. Dielectric dispersion. The variation of the real part of dielectric permittivity (ε') with frequency is termed the dielectric dispersion (figure 5). It can also be seen that the dielectric permittivity decreases continuously with increasing frequency. The greater the polarizability of the molecules, the higher is the permittivity of the material. The dispersion occurring in the lower frequency regime is attributed to interfacial polarization since the electronic and atomic polarizations remain by and large unchanged at these frequencies. As the size of the particle decreases to nanometric dimensions with increase in the volume fraction of the particles, interfacial polarization plays a major role in determining the dielectric properties of the material [15]. In the high frequency regime the decrease in the value of dielectric permittivity is very small. Any mechanism of polarization contributing to polarizability is observed to show lagging with the applied field at these frequencies. This can result in reduced polarization leading to diminished ε' values at higher frequencies.

Considering the ferrite system as a heterogeneous system with grains and grain boundaries possessing different conducting properties, the variation in dielectric permittivity can be viewed from a different perspective. The dielectric dispersion observed in a number of ferrite systems was explained satisfactorily on the basis of the Maxwell–Wagner theory of interfacial polarization [16] in consonance with the Koops phenomenological theory [17, 18]. According to this model, it is the conductivity of grain boundaries that contributes more to the dielectric value at lower frequencies. The variation of dielectric permittivity with frequency and temperature of $MnFe_2O_4$ prepared by the ceramic method was also carried out for a comparison. The variation of ε' of the ceramic sample is shown in figure 6. In the nano regime the number of grains and grain boundaries is large and hence a large dielectric permittivity is expected at low frequencies. Hence the observed enhancement in the dielectric permittivity in the nanosystem can be directly associated with the presence of numerous nanosized grains and interfaces. The dielectric value is found to vary inversely with frequency in our nanosystem. This is in tune with the Maxwell–Wagner theory. However there are also reports wherein deviation from the Maxwell–Wagner theory has been stated [15].

In ferrites it is observed that the mechanism of dielectric polarization is similar to the mechanism of electrical conduction. The variation of dielectric permittivity can hence

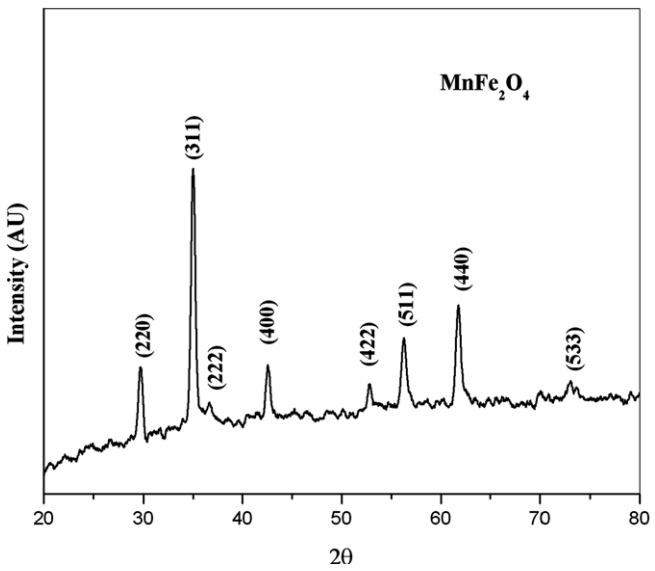

Figure 1. XRD pattern of co-precipitated $MnFe_2O_4$ powder.

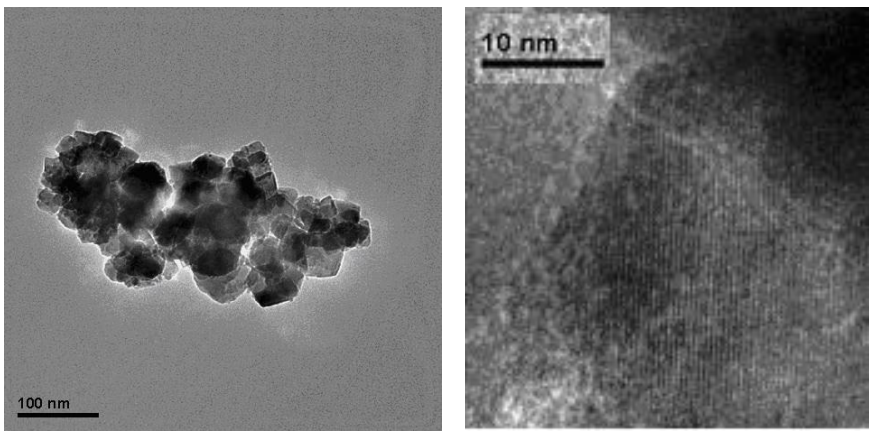

(a) (b)

Figure 2. TEM (*a*) and HRTEM (*b*) images of $MnFe_2O_4$ nanoparticles.

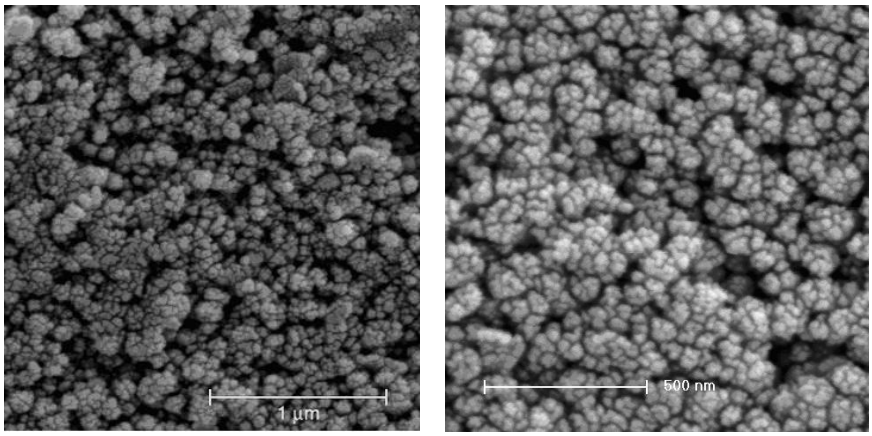

(a) (b)

Figure 3. SEM images of $MnFe_2O_4$ pellet.

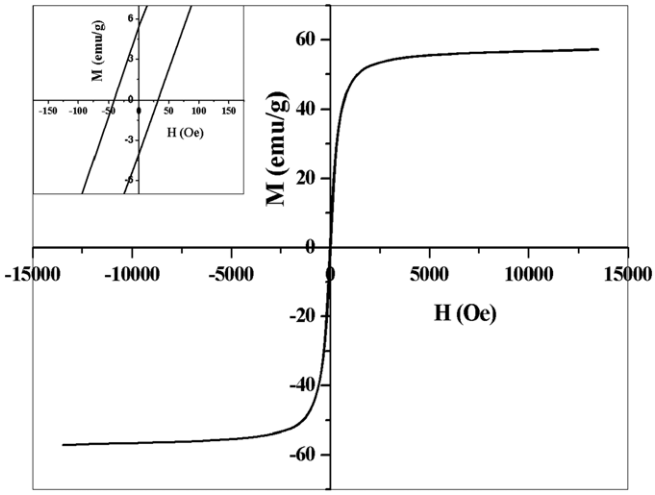

Figure 4. Room temperature M–H curve of co-precipitated $MnFe_2O_4$ powder. (Inset shows an expanded view of the hysteresis curve.)

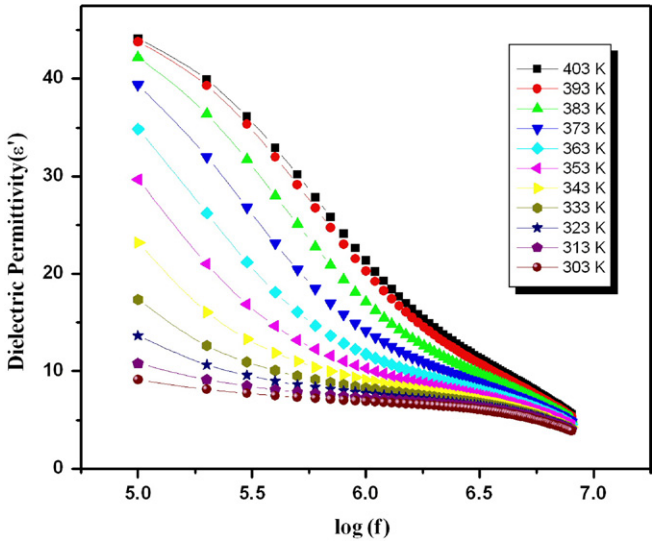

Figure 5. Dielectric dispersion of nanostructured $MnFe_2O_4$.

be related to the collective behaviour of both types of electric charge carriers, electrons and holes. This is explained on the basis of the Rezlescue model [19]. Applying this model, the electrons exchanging between Fe^{2+} and Fe^{3+} ions and the holes that transfer between Mn^{3+} and Mn^{2+} ions are responsible for electric conduction and dielectric polarization in manganese ferrite [20, 21]. At higher frequencies, the frequency of electron/hole exchange will not be able to follow the applied electric field, thus resulting in a decrease in polarization. Consequently, the dielectric permittivity remains by and large the same.

The temperature dependence of dielectric permittivity at selected frequencies is represented in figure 7. It can be seen that the value of ε' increases with increase in temperature. This type of behaviour was observed in a number of ferrites [22]. As temperature increases the orientation of dipoles is facilitated and this enhances the dielectric permittivity. At lower frequencies the rapid increase in dielectric permittivity with temperature is mainly due to interfacial and dipolar polarizations which are strongly temperature dependent. As temperature increases, the

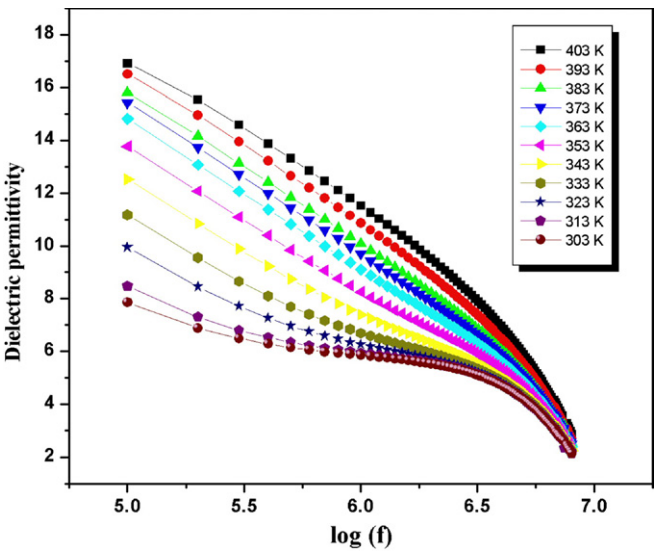

Figure 6. Dielectric dispersion of ceramic $MnFe_2O_4$.

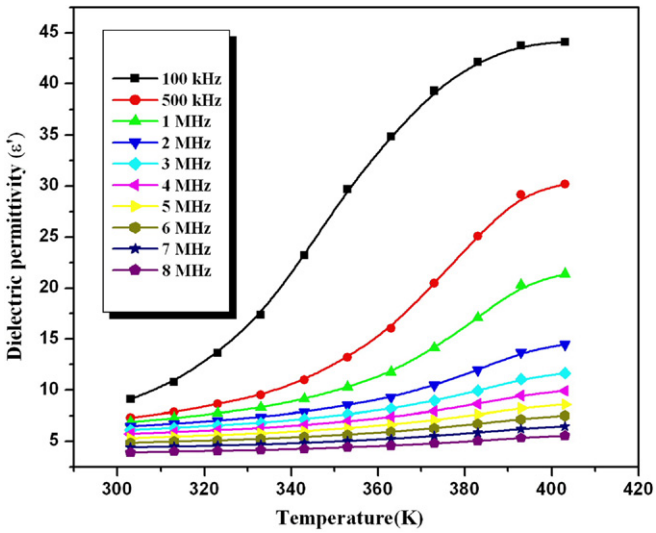

Figure 7. Variation of ε' with temperature in nanostructured $MnFe_2O_4$.

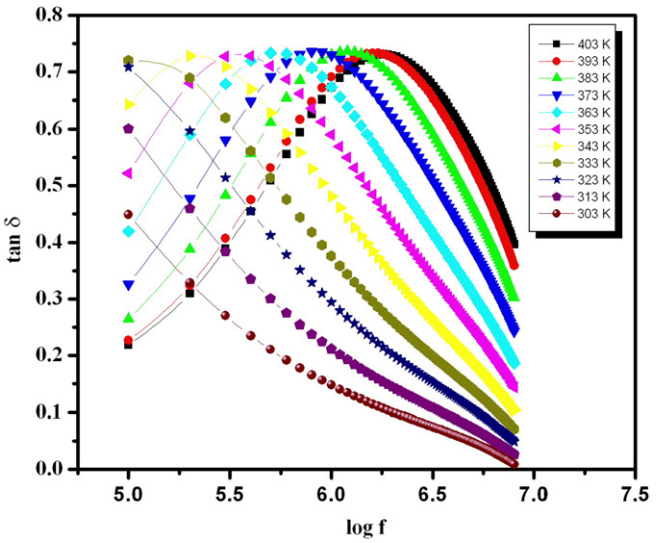

Figure 8. $\tan\delta$ versus $\log f$ of nanostructured $MnFe_2O_4$.

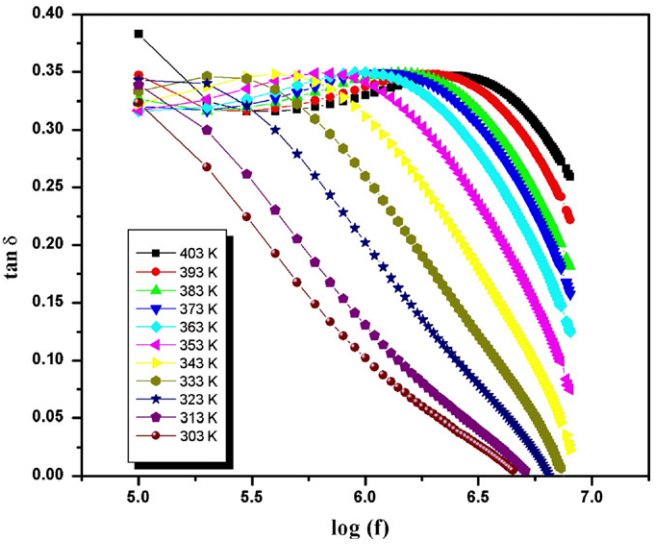

Figure 9. $\tan\delta$ versus $\log f$ of ceramic $MnFe_2O_4$.

accumulation of charges on the grain boundaries increases, which causes an increase in the interfacial polarization. This is at lower frequencies. Therefore the dielectric polarization increases, causing a marked difference in ε' with temperature. The relatively insignificant variation of dielectric permittivity with temperature observed at higher frequencies is attributed to atomic and electronic polarizations which are independent of both frequency and temperature.

On considering the dependence of dielectric permittivity with temperature, the results show that at lower frequencies the change in dielectric permittivity in the temperature range of 30–130 °C is 80%. However, at 8 MHz the change is of the order of only 5%. This is in accordance with the model of Haberey and Wijin on ferrites [23]. This can also be explained based on the Maxwell–Wagner theory. That is, the dielectric properties of ferrites in the lower frequency regime are determined solely by the grain boundary effect, which is highly temperature dependent.

3.2.2. Dielectric absorption. The variation of ε'' and $\tan\delta$ with frequency at various temperatures is shown in figures 8 and 10. Both ε'' and $\tan\delta$ showed a relaxation. No strong relaxation peaks were found in the case of the ceramic sample (figures 9 and 11). The presence of relaxation peaks in the nanostructured manganese ferrite is suggestive of the fact that a different relaxation process is occurring in the nanoregime. At the maxima, the oscillating charges are coupled directly with the oscillating field, which results in a maximum absorption of the electrical energy. In nanometre sized particles, the contribution of interfacial loss and the loss from electrical conductivity is not negligible but rather dominant at lower frequencies. But at higher frequencies these losses are minimum. This may be one of the reasons for the decrease in ε'' at higher frequencies.

In the frequency range of 100 kHz–8 MHz, $\tan\delta$ values vary between 0.75 and 0.005. Considering hopping conduction, it can also be said that dielectric relaxation occurs when the hopping frequency of the charge carriers becomes approximately equal to that of the external applied field. It is observed that as temperature is increased, the maximum value of relaxation for ε'' and $\tan\delta$ shifts towards [24] higher frequencies (figures 8 and 10). As temperature is increased, the hopping frequency of the charge carriers increases due to thermal activation and hence the maxima in the spectrum also shift [25].

The condition for observing a maximum in the dielectric loss of a dielectric material is given by the relation

$$\omega\tau = 1, \tag{4}$$

where τ is the relaxation time and $\omega = 2\pi f_{\max}$

The value of $f_{\max}$ can easily be observed from figure 8. The relaxation time τ can be determined from (4). Then τ can be written as

$$\tau = \tau_0 \exp\left(\frac{E_d}{k_B T}\right), \tag{5}$$

where τ_0 is the pre-exponential constant which equals the relaxation time at infinitely high temperatures, k_B is the

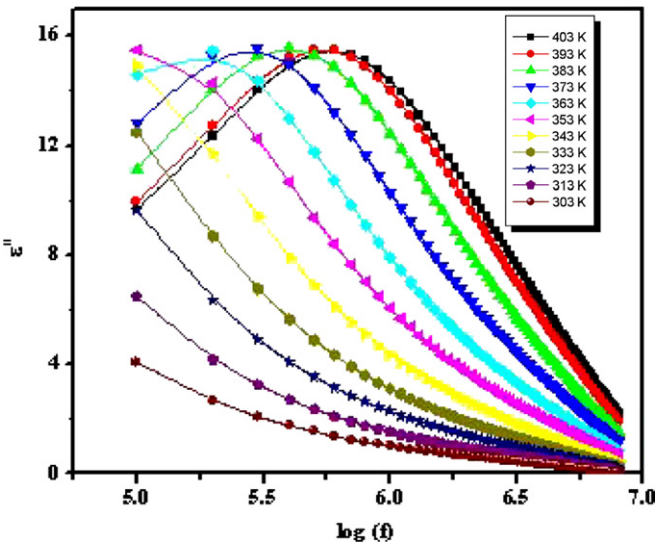

Figure 10. Dielectric absorption in nanostructured $MnFe_2O_4$.

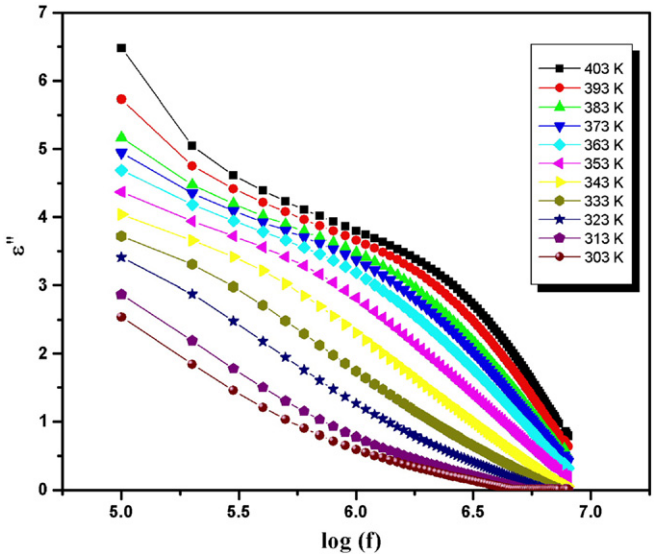

Figure 11. Dielectric absorption in ceramic $MnFe_2O_4$.

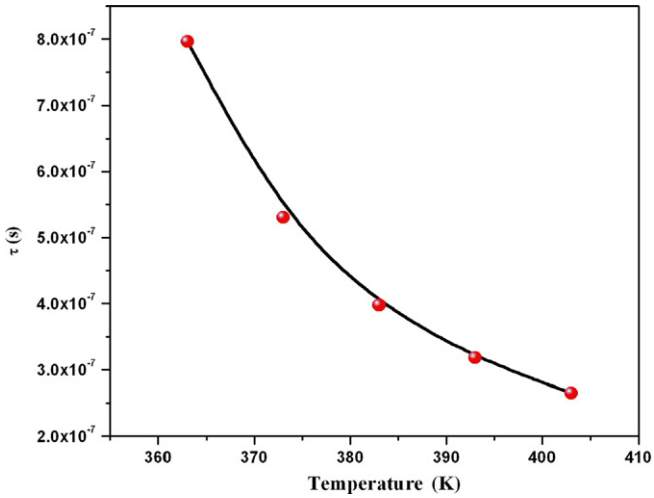

Figure 12. Variation of τ with temperature

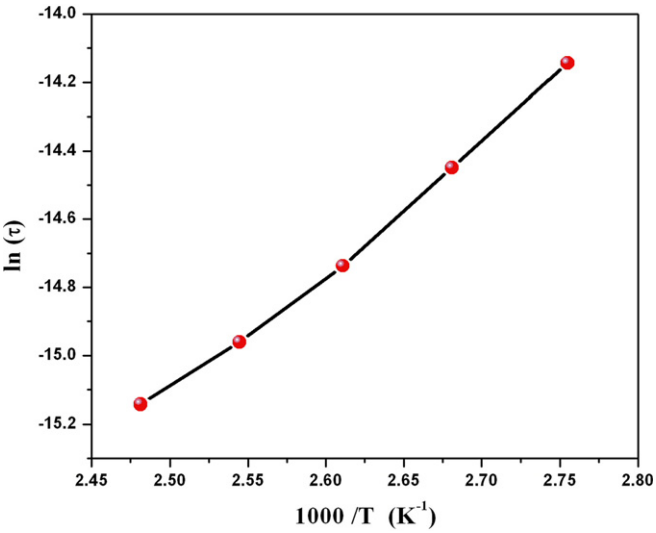

Figure 13. $\ln \tau$ versus $1000/T$ curve.

Boltzmann constant, T is the temperature in K and E_d the activation energy for dielectric relaxation.

The variation of τ with temperature is shown in figure 12. A decrease in relaxation time with temperature can be noted here. The possibility of the existence of multiple equilibrium states with a distribution of relaxation time in the nanosystem is thus evident here.

From the slope of the graph between $\ln \tau$ and $1000/T$, E_d the activation energy for dielectric relaxation can be determined (figure 13). The hopping depends on the activation energy which is associated with the electrical energy barrier experienced by the electrons during hopping. Since $\tau = 1/2P$, where P is the hopping probability, the decrease in relaxation time with temperature results in an increase in hopping probability with temperature [26]. The activation energy for dielectric relaxation in the high temperature region is found to be 0.337 eV. Large value of activation energy [27] and relaxation nature of dielectric loss suggest two distinct conduction processes, namely quantum mechanical tunnelling through the barrier separating the two equilibrium positions and classical hopping of a carrier over the barrier or some combination or a variant of the two and it can be assumed that electrons or polarons or ions are responsible for conduction.

3.3. Ac conductivity studies

The variation of ac conductivity with frequency and temperature is given in figure 14. It is observed that the ac conductivity first increases with frequency, reaches a maximum and then decreases. As the frequency of the applied field increases, the hopping of carriers also increases; thereby increasing the conductivity. But at higher frequencies the hopping of charge carriers could not follow the applied field frequency and it lags behind the applied frequency, resulting in a decrease in the ac conductivity values.

The increase in ac conductivity with frequency and temperature could also be explained on the basis of the Koops model. According to this model, low frequency conductivity

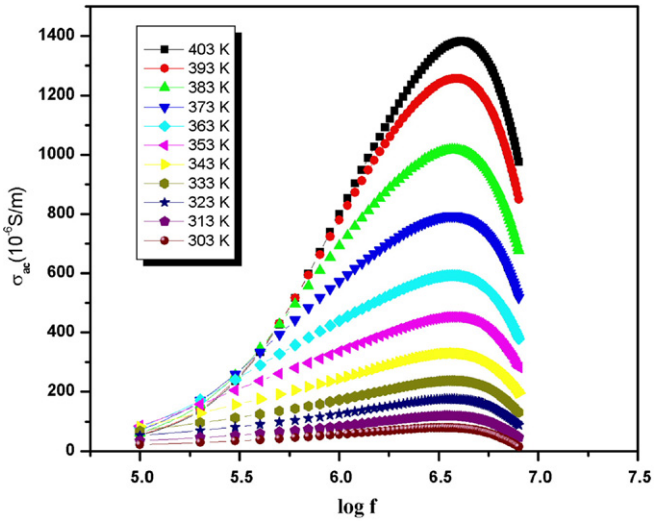

Figure 14. Variation of σ_{ac} with frequency in nanostructured $MnFe_2O_4$.

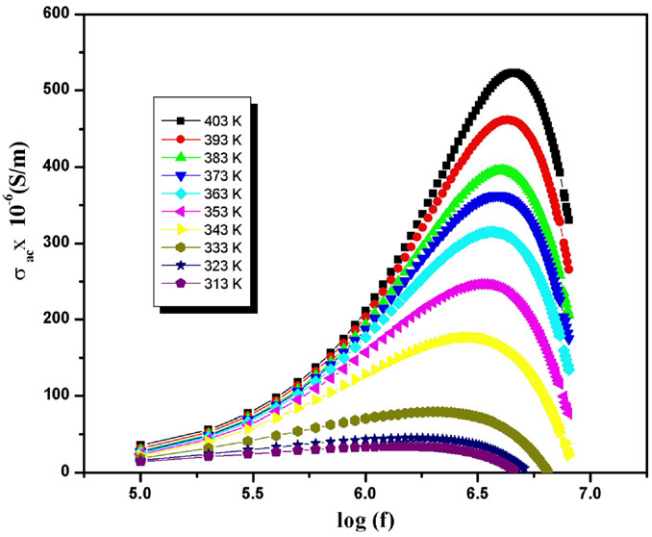

Figure 15. Variation of σ_{ac} with frequency in ceramic $MnFe_2O_4$.

is due to the grain boundaries, while the dispersion at higher frequencies is due to the conducting grains. Since the high density of interfacial states in the nanosystem can serve as charge carriers due to ionization and can also function as conduction centres for the transport of charge carriers, the ac conductivity in these systems is at variance with respect to the bulk and the conductivity is found to be higher. This is evident from the ac conductivity studies carried out on the ceramic sample of $MnFe_2O_4$ (figure 15).

The results of ac conductivity can also be explained on the basis of the assumption that the real ac electrical conductivity [28] consists of two terms

$$\sigma_{ac}(T) = \sigma_1(T) + \sigma_2(T). \tag{6}$$

The first term is the temperature dependent dc conductivity, which is related to the drift of electric charge carriers and

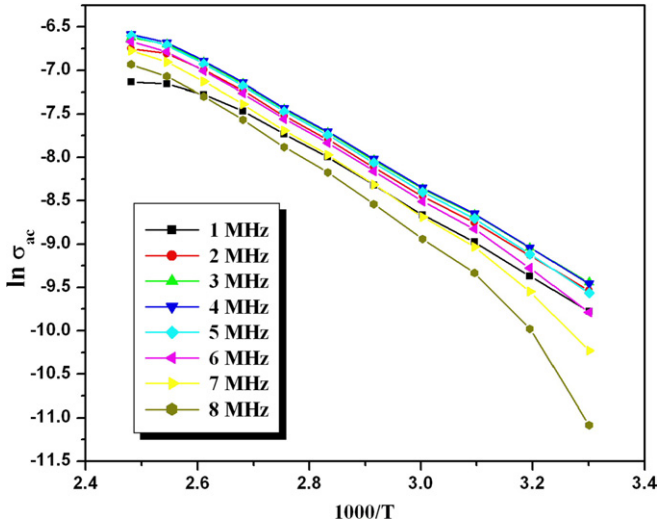

Figure 16. $\ln \sigma_{ac}$ versus $1000/T$ curve.

follows an Arrhenius relation given by

$$\sigma_1(T) = \sigma_0 \exp\left(-\frac{E_a}{k_B T}\right), \tag{7}$$

where E_a is the activation energy for electric conduction, σ_0 is the pre-exponential factor.

The second term is the temperature and frequency dependent part, which is related to the dielectric relaxation caused by the localized electric charge carriers. The power law is given by [29]

$$\sigma_2(\omega, T) = B(T)\omega^n(T), \tag{8}$$

where B is a parameter having unit of conductivity and n is a dimensionless parameter.

The activation energy at different frequencies can be found by plotting $\ln \sigma_{ac}$ versus temperature (from equation (7)). From the slope of the linear region, activation energy (E_a) for electrical conduction at different frequencies was estimated and is shown in figure 16.

The activation energy is found to be decreasing with frequency up to around 4 MHz (figure 17). Above this region an increase in activation energy is observed for frequencies where the hopping of charge carriers lags behind the applied frequency. Thus it can be assumed that ac conductivity is due to the polaron conduction mechanism, which is both frequency and temperature dependent. The polarons tend to relax at frequencies below the hopping frequency. From the hopping frequencies of the polarons, the relaxation times are evaluated. As the temperature increases, the polarons have sufficient thermal energy to get activated and jump over the barrier or tunnel through the barrier. Since ac conductivity is frequency dependent, the power law ($\sigma(\omega, T) = B\omega^n(T)$) can be applied to the experimental data by plotting $\log \sigma_{ac}$ with $\log \omega$ (figures 18(a) and (b)). They exhibit logarithmic dependence of frequency at different temperatures (303–333 K) and (343–403 K). We obtained straight lines with a slope equal to n and an intercept equal to $\log B$ on the vertical axis at $\log \omega = 0$.

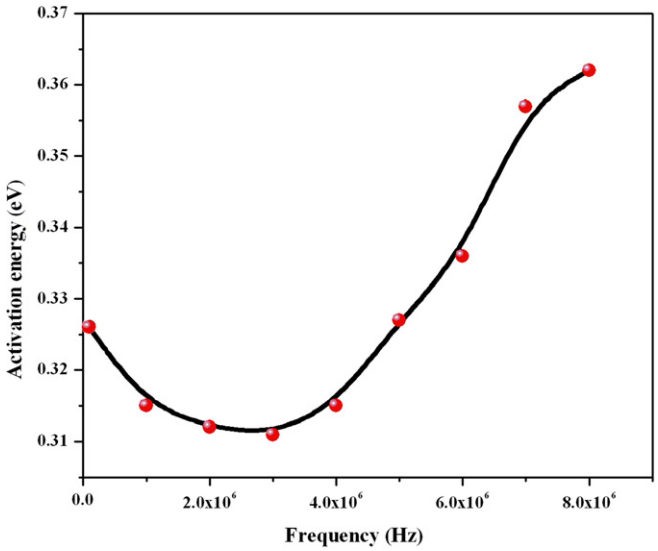

Figure 17. Variation of activation energy with frequency.

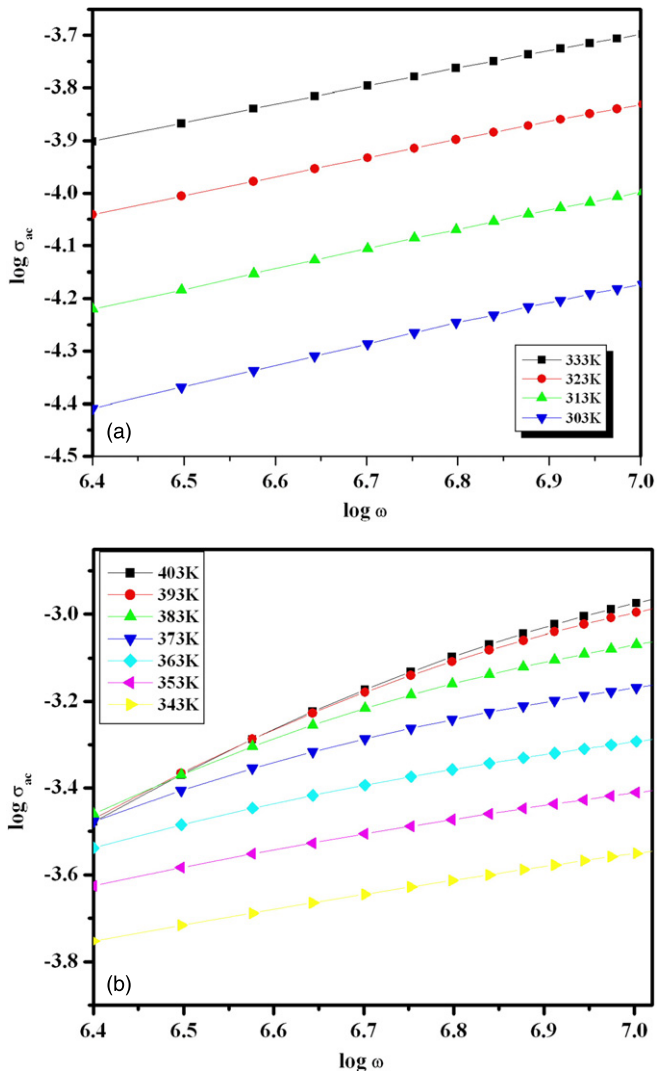

Figure 18. Plot of $\log \sigma_{ac}$ versus $\log \omega$ for the two temperature ranges. (*a*) 303–333 K and (*b*) 343–403 K.

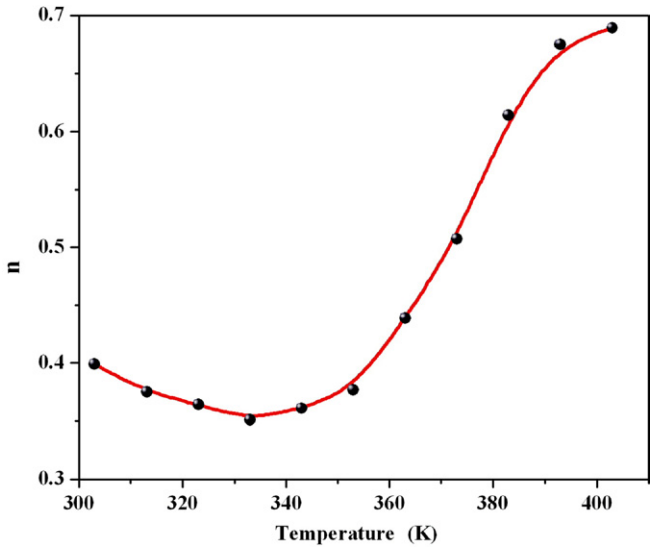

Figure 19. Variation of n with temperature.

The value of n thus obtained from the graph decreases from 0.399 to 0.351 with increase in temperature in the range 303–333 K and increases from 0.351–0.689 with increase in temperature in the range 343–403 K (figure 19). It is known that a study of the variation of n with temperature can throw light on the conduction mechanism [30,31]. If n increases with the temperature, small polaron conduction is predominant [32]. A minimum value of n followed by an increase suggests that the conduction mechanism is due to an overlapping large polaron tunnelling mechanism [33]. In the case where n is temperature independent, quantum mechanical tunnelling is expected [34]. The correlated barrier hopping is usually associated with a decrease in n with temperature [35]. In this investigation the variation of n indicates the possibility of an overlapping large polaron tunnelling mechanism (OLPT).

In the OLPT model, Long has proposed a mechanism for polaron tunnelling where the polaron energy is derived from polarization changes in the deformed lattice [36]. The resultant excitation is called a large polaron. Because of long range Coloumb interaction, the potential well of a site will extend over many interatomic distances and overlap with the well of other sites. Then the activation energy of the sites will be reduced according to the relation

$$W_{\mathrm{H}} = W_{\mathrm{HO}}[1 - r_{\mathrm{p}}/R], \tag{9}$$

where r_{p} is the polaron radius and R is the intersite separation and W_{HO} is given by

$$W_{\mathrm{HO}} = \frac{e^2}{4\varepsilon_{\mathrm{p}} r_{\mathrm{p}}}, \tag{10}$$

where ε_{p} is the effective dielectric constant. It is assumed that W_{HO} is constant for all sites while R is a random variable.

By the OLPT model, ac conductivity is given as

$$\sigma_{\mathrm{ac}}(\omega) = \frac{\pi^4}{12} e^2 (k_{\mathrm{B}}T)^2 [N(E_{\mathrm{F}})]^2 \frac{\omega R_\omega^4}{(2\alpha k_{\mathrm{B}}T + (W_{\mathrm{HO}} r_{\mathrm{p}}/R_\omega^2))}, \tag{11}$$

where k_B is the Boltzmann constant, T is the temperature in degree absolute, α the spatial extent of the polaron, $N(E_F)$ the density of states at the Fermi level and R_ω is the tunnelling distance.

R_ω, the tunnelling distance at a frequency ω, is determined by the quadratic equation

$$R_\omega'^2 + [\beta W_{HO} + \ln(\omega\tau_0)]R_\omega' - \beta W_{HO} r_p = 0, \qquad (12)$$

where $R_\omega' = 2\alpha R_\omega$, $r_p' = 2\alpha r_p$ and β is $1/k_B T$.

The frequency exponent n is evaluated from equations (8), (11) and (12) as,

$$n = 1 - \frac{8\alpha R_\omega + (6\beta W_{HO} r_p / R_\omega)}{(2\alpha R_\omega + (\beta W_{HO} r_p / R_\omega))^2}. \qquad (13)$$

The frequency exponent n initially shows a decrease with temperature, then reaches a minimum and then increases. A similar variation is observed in the present system of manganese ferrite nanoparticles. The polaron formation in the nano ferrite system can be due to the defect levels present at the nanolevel. The multiple valence states of Mn (Mn^{2+} and Mn^{3+}) in the system point towards possible Jahn–Teller distortion occurring in the system resulting in the creation of defects which can facilitate polaron formation. The decrease in conductivity after a particular frequency suggests frequency dependent polaron conduction, which decreases at higher frequencies. However, a detailed theoretical study is essential to explore the different aspects of this type of conduction mechanism in nanostructured manganese ferrite.

4. Conclusion

Nanosized $MnFe_2O_4$ was prepared by employing co-precipitation techniques. The saturation magnetization of nanosized manganese ferrite was found to be less than that of its bulk counterpart. The variation of dielectric permittivity, loss factor and ac conductivity values with frequency and temperature was studied in detail. The variation was explained based on the Maxwell–Wagner theory of interfacial polarization in consonance with Koops phenomenological theory. Activation energy for dielectric relaxation was evaluated from the dielectric absorption measurements and it is suggestive of polaron hopping or tunnelling. The distribution of relaxation time provides enough evidence for the existence of multiple equilibrium states in the system. For comparison a manganese ferrite prepared by ceramic techniques was also subjected to similar dielectric studies. The studies indicate that nanostructured manganese ferrite exhibits enhanced dielectric properties compared with the ceramic. The variation of frequency exponent n with temperature in the frequency dependent ac conductivity component ($\sigma(\omega, T) = B\omega^n(T)$) is indicative of overlapping large polaron tunnelling conduction in manganese ferrite in the nanoregime. These investigations suggest that the properties of nanostructured $MnFe_2O_4$ ferrite can be manipulated for suitable applications. Scope exists for studies on similar nanostructured mixed ferrites.

Acknowledgments

EVG acknowledges Cochin University of Science and Technology for the Research Fellowship. MRA acknowledges AICTE, Government of India (Centre for Ferrofluids, File No 8023/RID/RPS-73/2004-05. Dated 29/03/2005), for the financial assistance. KAM thanks the Department of Science and Technology for financial assistance received under WOS-A Project (No SR/WOS-A/PS-94/2003).

References

[1] Sugimoto M 1999 *J. Am. Ceram. Soc.* **82** 269
[2] Gillot B 2002 *Eur. Phys. J.: Appl. Phys.* **91** 10
[3] Somiya S, Aldinger F, Claussen N, Spriggs R M, Uchino K, Koumoto K and Kaneno M 2003 *Handbook of Advanced Ceramics* vol 2 (London: Academic) p 187
[4] Pankhurst Q A, Connolly J, Jones S K and Dobson J 2003 *J. Phys. D: Appl. Phys.* **36** R167
[5] Vishwanathan B and Moorthy V R K 1990 *Ferrite Materials: Science and Technology* (Berlin: Springer)
[6] Sakurai J and Shinjo T 1967 *J. Phys. Soc. Japan* **23** 1426
[7] Flatemi D J, Harris V G, Chen M X, Malik S K, Yelon W B, Long G J and Mohan A 1999 *J. Appl. Phys.* **85** 5172
[8] Tang Z X, Sorenson C M, Klabunde K J and Hadjipanayis G C 1991 *Phys. Rev. Lett.* **67** 3602
[9] Chen J P, Sorenson C M, Klabunde K J, Hadjipanayis G C, Delvin E and Kostikas A 1996 *Phys. Rev.* B **54** 9288
[10] Zhang Z J, Wang Z L, Chakoumakos B C and Yin J S 1998 *J. Am. Chem. Soc.* **120** 1800
[11] Denecke M A, Ber W G, Buxbaum G and Kuske P 1992 *Mater. Res. Bull.* **27** 507
[12] Shenoy S D, Joy P A and Anantharaman M R 2004 *J. Magn. Magn. Mater.* **269** 217
[13] George M, John A M, Nair S S, Joy P A and Anantharaman M R 2006 *J. Magn. Magn. Mater.* **302** 190
[14] Sindhu S, Anantharaman M R, Thampi B P, Malini K A and Kurian P 2002 *Bull. Mater. Sci.* **25** 599
[15] George M, Nair S S, Malini K A, Joy P A and Anantharaman M R 2007 *J. Phys. D: Appl. Phys.* **40** 1593
[16] Wagner K W 1913 *Ann. Phys.* **40** 817
[17] Koops C G 1951 *Phys. Rev.* **83** 121
[18] Miles P A, West Phal W B and Von Hippel A 1957 *Rev. Mod. Phys.* **29** 279
[19] Rezlescu N and Rezlescu E 1974 *Phys. Status Solidi* a **23** 575
[20] Ravinder D and Latha K 1994 *J. Appl. Phys.* **75** 6118
[21] Abdeen A M 1999 *J. Magn. Magn. Mater.* **192** 121
[22] Shaik A M, Bellad S S and Chougule B K 1999 *J. Magn. Magn. Mater.* **195** 384
[23] Haberey H and Wijin H 1968 *Phys. Status Solidi* a **26** 231
[24] Abo El Ata A M and Attia S M 2003 *J. Magn. Magn. Mater.* **257** 165
[25] Zaki H M 2005 *Physica* B **363** 232
[26] Reddy B and Reddy P V 1991 *Physica* D **24** 975
[27] Klinger M I 1975 *J. Phys. C: Solid State Phys.* **8** 3595
[28] Ahmed M A, El Hiti M A, El Nimr M K and Amer M A 1996 *J. Magn. Magn. Mater.* **152** 391
[29] El Hiti M A 1996 *J. Phys. D: Appl. Phys.* **29** 501
[30] Elliot S R 1987 *Adv. Phys.* **36** 135
[31] Fayek M K, Mostafa M F, Sayedahmed F, AtaAllah S S and Kaiser M 2000 *J. Magn. Magn. Mater.* **210** 189
[32] Meaz T M, Attia S M and Abo El Ata A M 2003 *J. Magn. Magn. Mater.* **257** 296
[33] Ghosh A 1990 *Phys. Rev.* B **42** 1388
[34] Austin I G and Mott N F 1969 *Adv. Phys.* **19** 41
[35] Elliot S R 1977 *Phil. Magn.* **36** 12
[36] Long A R 1982 *Adv. Phys.* **31** 553